ORIGINAL

CrossMark

Numerical analysis on thermal energy storage device to improve the drying time of indirect type solar dryer

Satyapal Yadav[1] · Abhay Bhanudas Lingayat[1] · V.P. Chandramohan[1] · V. R. K. Raju[1]

Abstract

Thermal energy storage (TES) device that uses phase change material (PCM) in the field of indirect solar drying is economical due to its energy storage characteristics. In this work, a low-temperature latent heat TES device has been numerically analyzed for the application of solar drying of agricultural products in an indirect type solar dryer. Paraffin wax is used as a PCM material. The study has been performed on a single set of concentric tubes which consist of an inner copper tube and an outer plastic tube. A 2D geometry is created and computational fluid dynamics (CFD) simulations are performed using ANSYS Fluent 2015. The hot air coming from solar collector enters the copper tube and then the drying chamber to dry the sample. PCM material is placed in the outer plastic tube. It was found that the drying process can be continued up to 10.00 pm without further source of heating. At a given time, the melting fraction is increased during the heating process and solidification factor is increased during the cooling process while increasing the air flow velocities from 1 to 4 m/s, but 1 m/s is good for maintaining outlet temperature of air (T_{oa}) for a long time. Heat lost and gained by air was estimated. It was found that air flow velocity influenced the heat lost and gain by air.

Nomenclature

A	area of contact wall (m^2)
C_p	specific heat (J/kg K)
CVs	control volumes
H	Enthalpy (J/kg)
h	heat transfer coefficient (W/m^2 K)
k	thermal conductivity (W/m K)
L	latent heat of fusion (J/kg)
PCM	phase change material
p	pressure (Pa)
TES	thermal energy storage
T	temperature (K)
t	time (s)
u, v	velocity (m/s)
r, y	coordinates (m)

Greek symbols

β	thermal expansion coefficient (1/K)
ρ	Density (kg/m^3)
μ	Dynamic viscosity (kg/m s)
γ	melting fraction

Subscripts

a	air, ambient
ac	air with copper wall
c	copper
i	inlet
L	Latent
li	liquid
m	melting
o	outlet
p	PCM
pc	PCM with copper wall
ref.	reference
s	solid
S	Sensible
w	wall

✉ V.P. Chandramohan
vpcm80@nitw.ac.in

[1] Mechanical Engineering Department, National Institute of Technology Warangal, Warangal, Telangana 506004, India

1 Introduction

Energy consumption for drying constitutes a major component of energy consumption in developing countries. The consumption of fossils fuels is reduced if solar energy is used to dry food grains, fruits, vegetables, medicinal plants and other edible and non-edible seeds. Thermal energy is stored in the

🖄 Springer

form of sensible heat and latent heat. It can be stored also in the form of chemical energy. When the temperature rises in the thermal storage material, energy is stored in the form of sensible heat. Materials like fire bricks, sand, limestone etc. are solid state sensible heat storage materials. Materials like paraffin wax, formic acid, glycerin etc. are used as a phase change material to store latent heat. Availability of solar energy is not consistent throughout the day. A temperature range of 323 K to 348 K is needed for many hours and in some cases, it is needed for 2 to 3 days at a stretch for the safe drying of agricultural products. Thermal energy storage (TES) by phase change materials (PCM) [1] is one of the viable options to overcome the above issue and to enhance the drying operation. In the solar dryer setup with PCM, excess energy is stored during the peak time of solar radiation and it is utilized at an off-sun time or when sufficient solar radiation is not available. The application of TES in drying is an economical method [2]. Several methods have been implemented to improve the performance of indirect solar dryer for drying of food products. Some of them are discussed below:

Shalaby et al. [1] designed a novel indirect solar dryer provided with paraffin wax as a phase change material (PCM) as energy storage medium and experimentally investigated the performance of the dryer with PCM and without PCM. From the experimental results, it was concluded that PCM helped to maintain the uniform drying temperature in the chamber at an approximately constant value for 7 consecutive hours a day.

Zhao et al. [2] numerically analyzed PCM with graphite foam for applications in high-temperature latent heat storage systems of concentrated solar power plants. Magnesium chloride ($MgCl_2$) was chosen as PCM for the TES system whose melting point was 987 K. Heat transfer performance in the storage tank was analyzed with the anisotropic thermal conductivity and 3-D numerical simulations were performed using commercial software COMSOL. The plant electricity generation capacity was set at 100 MW with 12 h storage capacity. It was found that the graphite foam considerably improved the thermal performance of the latent heat TES system.

Ayyappan et al. [3] developed an experimental setup for tunnel shaped indirect type solar dryer with sensible heat storage materials. Different materials such as sand, rock and concrete were used as heat storage materials. They found that the use of concrete as heat storage material gave better day time temperature (16 °C more than ambient temperature) and night time temperature of 3 °C more than the ambient temperature. Sand increased the day and night time temperatures of 12 and 3.5 °C more than ambient temperature, respectively. Coconut has been used as sample material during drying experiments and it lost its moisture content from 52 to 7.5 kg/kg of wet basis.

An experimental setup for efficient and cost effective solar dryer was developed by Baniasadi et al. [4]. It was developed with a forced convection facility and thermal energy storage system. Drying experiments were carried with fresh apricot slices. It was concluded that the system performance was increased and the drying time was increased while using thermal energy storage system.

Cakmak et al. [5] experimentally investigated a novel type of solar dryer to evaluate the drying kinetics of seeded grapes. The dryer consisted of a solar air collector, drying chamber and another collector with a PCM. The dimension of solar collector was $0.94 \times 1.85 \times 0.2$ m^3. Turbulence was created by making 15 mm diameter holes on the expanded surface collector. Another collector was included with PCM for drying grapes within a certain drying time and carrying out the drying process even after sunset. PCM used in the lower section of solar collector was calcium chloride hexahydrate. The air was forcefully passed through storage collector (with PCM collector) after sunset by a fan.

Tekasakul et al. [6] developed an experimental setup for rubber sheet drying with energy storage materials. The energy storage unit produced air temperature from 40 to 60 °C and therefore, their wood input to the furnace was reduced. Brick was used as the effective energy storage material and the effect of height of brick stack was analyzed against the thermal efficiency of energy storage system. They [6] found that the thermal efficiency was varied from 28 to 33% when the height of brick stack was varied from 50 to 150 cm. The drying time was also reduced to 78 h in this setup with energy storage facility compared to other conventional dryers of 120 to 148 h. They found that the natural color of rubber sheets were retained using this setup compared to other fire wood conventional dryers.

A numerical analysis was performed by Arsau et al. [7] for the melting of paraffin wax with 2% Al_2O_3 as a nano-PCM in a square enclosure. It was observed that effective thermal conductivity of paraffin wax latent heat storage medium was significantly increased by using smaller volumetric concentration of alumina particles in paraffin wax. Similar numerical analysis was performed by Lafdi et al. [8] with the PCM of graphite foams for space and terrestrial applications. They found that the power output was 97%, which was 5 times higher than pure PCM. Also, it is found that the porosity of PCM (graphite foam) couldn't make much impact on power output of the system. A review work was carried out by Dutil et al. [9] on PCMs and their implication on power demand. They suggested that latent heat storage systems and their application involving PCMs are becoming more attractive for space heating and cooling in buildings, solar applications (drying, medicine room etc.), off-peak energy storage and heat exchanger improvements. This work listed the various organic and inorganic PCMs' thermal properties such as melting and freezing temperature, density, specific heat and latent heat

energy. Another review work was carried out by Sharma and Sagara [10] which concluded that selection of appropriate PCM makes a huge impact on heat transfer problems. This work suggested selecting organic PCMs for food drying applications. It also tabulated the merits and demerits of different PCMs used for engineering applications.

Khodadadi et al. [11] studied numerically the impact of PCMs with nano-particle for improved thermal energy storage. They considered buoyancy-driven convection in a differentially heated cavity containing a nanofluid. The cavity was filled with nanofluid particles (water and copper). The boundary condition of the cavity was adiabatic at top and bottom surface and isothermal at the left and right wall. They predicted the heat extraction rate during the solidification process.

Karunesh et al. [12] numerically solved the problem of melting for paraffin (PCM) by commercial software COMSOL 5.0 based on finite element method. The problem domain was a 2 D rectangular aluminum cavity with the boundary conditions of one side being isothermal temperature and the rest being insulated sides. Performances of five different PCMs (fatty acids such as Capric acid, Lauric acid, Myristic acid, Palmitic acid and Stearic acid) were studied and compared with the paraffin. The results were reported in terms of melt fraction, temperature variation, transition of solid-liquid interface and the quantity of thermal energy stored in different fatty acids with time for melting and solidification. It was found that the maximum energy was stored in Stearic acid and minimum was in Capric acid. It showed that selection of proper PCM was important for the particular application.

From the literature survey, it is noticed that the PCMs overcome the energy demand after sunset and it stores excess energy during day time. It is one of the safest sources of energy. PCMs are mainly classified into organic and inorganic, among that organic PCMs are chemically stable, it melts congruently and most of them are recyclable [9]. For the food drying applications, an appropriate PCM should be selected based on the temperature range of 30 to 70 °C, as beyond this temperature range, the food may be partially or fully cooked. Also, the selected PCM should be non-toxic and chemically stable, since it is for food drying applications. Therefore paraffin wax is selected for this numerical work as it is easily available and economical. It has a high heat of fusion per unit weight. This is non-toxic in melting and cooling (toxic only in burning). Paraffin PCM's also has a low thermal conductivity and can be re-cycled for further applications [9].

There are few works [6–8] that have discussed property enhancement of PCMs. There are some review works on solar dryer [3]. Very few works [9, 10, 13] concentrated only on PCMs and their improvement on heat transfer problems. The heat storage capacity of PCMs can be improved by fin-like structure in TES device or by adding some additives in PCM [3, 7]. Few works are available [1, 3, 5, 14, 15] on drying of agricultural products through solar energy. There are some

works contributed on convective drying [16–19] and freeze drying [20] of food products. There is limited numerical work on PCMs with different applications [6, 7, 12], and very few work [3, 5] carried out on drying of agricultural products with TES device. Melting and solidification factors of PCM are not discussed in any literature in the specific area of drying of food products in solar dryer set up, as they are necessary for determination of charging and discharging of thermal energy during drying. The effect of air flow velocity was not discussed in any of the work. Heat lost and gained calculations were not found in any literature. Therefore, the objectives of the present numerical work are; (i) to develop a numerical model for a low-temperature application thermal energy storage device for an indirect type solar dryer (ii) to estimate the melting and solidification fraction at different velocities, (iii) to determine temperature distribution of PCM during heating and cooling at different time, so that charging and discharging of thermal energy in PCM material during the process can be identified (iv) to develop the melting and solidification fraction contours for the system and (v) to estimate the heat lost and gained by air during the process at different air flow velocities.

2 Methodology

2.1 Geometry

Preliminary simulations were performed for plastic tube (which contains PCM) with diameters of 42, 37 and 32 mm for estimating the melting fraction (results not shown here). From the preliminary simulations the diameter of the plastic tube was selected as 32 mm such that melting completes at 2.00 pm on normal conditions of the day.

The PCM container (Fig. 1 a) consists of copper tubes (inner) for air flow and plastic tubes (outer) for PCM storage. The copper and plastic pipes are fitted in a concentric manner. The diameter of copper tube is 10 mm and its thickness is 1 mm. The diameter of outer plastic tube is 32 mm. The height of PCM container is set as 300 mm. For the present work, a 2D geometry is created axis-symmetrically for a single set of inner copper tube and outer plastic tube and it is shown in Fig. 1 (b). It is assumed that the outer tube consists of PCM material (paraffin wax) and the air flows inside the copper tube. Assuming longitudinal vertical axis and therefore, the horizontal width of air section is 10 mm.

2.2 Governing equations

The velocity and temperature distribution inside the copper tube should be estimated at different time as solar radiation is dependent on time. Therefore, in this problem the transient 2D cylindrical governing equations are taken for CFD simulations. The governing equations are:

Fig. 1 (a) Overall view of PCM container and (b) 2D view of copper and plastic concentric tubes
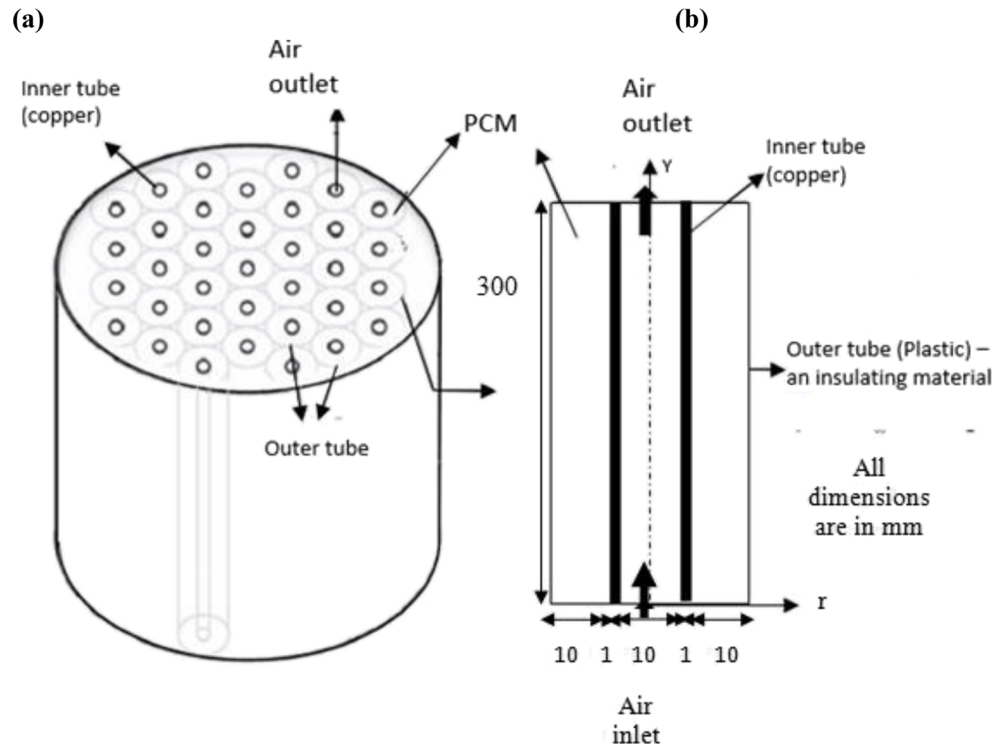
2.2.1 Conservation of mass (continuity equation)

$$\frac{\partial \rho}{\partial t} + \frac{1}{r}\frac{\partial(r\rho u_r)}{\partial r} + \frac{\partial(\rho v_y)}{\partial y} = 0 \tag{1}$$

2.2.2 Conservation of linear momentum in r and y component

$$\frac{\partial(\rho u_r)}{\partial t} + u_r\frac{\partial(\rho u_r)}{\partial r} + v_y\frac{\partial(\rho u_r)}{\partial y}$$
$$= -\frac{\partial p}{\partial r} + \frac{1}{r}\frac{\partial}{\partial r}\left(r\frac{\partial(\mu u_r)}{\partial r}\right) - \frac{u_r}{r^2} + \frac{\partial}{\partial y}\left(\frac{\partial(\mu u_r)}{\partial y}\right) \tag{2}$$

$$\frac{\partial(\rho v_y)}{\partial t} + u_r\frac{\partial(\rho v_y)}{\partial r} + v_y\frac{\partial(\rho v_y)}{\partial y}$$
$$= -\frac{\partial p}{\partial y} + \frac{1}{r}\frac{\partial}{\partial r}\left(r\frac{\partial(\mu v_y)}{\partial r}\right) + \frac{\partial}{\partial y}\left(\frac{\partial(\mu v_y)}{\partial y}\right) \tag{3}$$

2.2.3 Conservation of energy

$$\frac{\partial(\rho C_p T)}{\partial t} + u_r\frac{\partial(\rho C_p T)}{\partial r} + v_y\frac{\partial(\rho C_p T)}{\partial y}$$
$$= \frac{1}{r}\frac{\partial}{\partial r}\left(r\frac{\partial(kT)}{\partial r}\right) + \frac{\partial}{\partial y}\left(\frac{\partial(kT)}{\partial y}\right) \tag{4}$$

Where, u and v are velocity components in r and y directions respectively, p is pressure, t is time and T is temperature. The properties of air such as density (ρ), specific heat (C_p), viscosity (μ) and conductivity (k) are temperature dependent properties. The temperature of air is always changing from 293 to 373 K, therefore variation of properties was taken as piece wise linear profile and the values are tabulated in Table 1.

Enthalpy of PCM is computed from the sum of sensible heat (H_S) and effective latent heat (H_L).

Total enthalpy of material (H) and it is estimated as:

$$H = H_S + H_L \tag{5}$$

$$H_S = H_{ref} + \int_{T_{ref}}^{T} C_p (dT) \tag{6}$$

γ is the melting fraction and can be defined as,

$$\begin{aligned} &\gamma = 0; \text{if } T < T_s \\ &\gamma = 1; \text{if } T > T_{li} \\ &\gamma = \frac{T - T_s}{T_{li} - T_s}; \text{if } T_s < T < T_{li} \end{aligned} \tag{7}$$

Where, T_s and T_{li} are solid and liquid PCM temperature in K. Liquid temperature of PCM is the melting point temperature and solid temperature is always less than the melting point temperature of PCM. The region $0 < \gamma < 1$ is known as mushy zone region, the region where solid and liquid phase coexist.

The effective latent heat (H_L) is estimated from,

$$H_L = \gamma L \tag{8}$$

Table 1 Properties of air used for this simulation at different temperature [21]

Temperature (K)	Density (kg/m³)	Thermal conductivity (W/m K)	Dynamic viscosity (Pa s) 10^{-6}	Specific heat (J/kg K)
293	1.205	0.0257	18.207	1005
313	1.127	0.0271	19.125	1005
333	1.067	0.0285	20.166	1009
353	1.000	0.0299	20.940	1009
373	0.946	0.0314	21.814	1009

Where, L is latent heat of fusion in J/kg. The solidification and melting fraction are identified based on the temperature distribution of PCM. For estimating the temperature distribution of PCM, the energy equation is solved on the PCM region.

The PCM stores both sensible and latent heat. While estimating the temperature distribution of PCM material, both the sensible and latent heat should be accounted for. The energy equation is considered with both sensible heat and latent heat and can be written as:

$$\frac{\partial(\rho H)}{\partial t} + u\frac{\partial(\rho H)}{\partial r} + v\frac{\partial(\rho H)}{\partial y}$$
$$= \frac{1}{r}\frac{\partial}{\partial r}\left(rk\frac{\partial T}{\partial r}\right) + \frac{\partial}{\partial y}\left(k\frac{\partial T}{\partial y}\right) \tag{9}$$

Where H is total enthalpy and it is estimated from Eq. (5), u and v are fluid velocity in r and y directions, k is thermal conductivity of PCM, ρ is density of PCM which is a function of temperature [22] and it is expressed as,

$$\rho = \rho_s = 814 \text{ kg/m}^3; \text{if } 297 \text{ K} < T < T_m,$$
$$\rho = \rho_{li} = 775 \text{ kg/m}^3; \text{if } T = T_m,$$
$$\rho = \frac{\rho_{li}}{\beta(T-T_m)+1}; \text{if } T_m < T < 373K \tag{10}$$

Where, β is thermal expansion coefficient and T_m is melting point temperature of PCM.

Other properties of PCM, paraffin wax considered in this work, are mentioned in Table 2.

The following assumptions are used for solving the equations.

- There exists unsteady state heat transfer condition.
- There is laminar flow of air.
- The effect of buoyancy-driven convection is considered in the liquid phase PCM.
- The thermophysical properties of plastic (outer wall) are independent of temperature.
- Properties of air are a function of temperature and taken as piece-wise linear during heating (charging) and cooling (reuse or discharging) applications.
- PCM is homogeneous and isotropic.
- Mass flow rate of air is assumed to be constant.
- The outer wall of plastic tube is insulated.

2.3 Boundary and initial conditions

The calculation is started from 8.00 am. Therefore, the initial conditions used in this work are,

At time, $t = 0$; $v = 1$ m/s (air velocity at inlet), the ambient air temperature, $T_a = 308$ K.

2.3.1 Boundary condition at copper wall

$$h_{ac}A[T_w - T_a] = k_c A\frac{dT}{dr} + h_{pc}A[T_p - T_w] \tag{11}$$

Where, h_{ac} and h_{pc} are heat transfer coefficients of air with copper wall and PCM with copper wall, respectively. The first term of Eq. (11) gives the heat loss / gain of air from copper wall, second term represents the conduction heat transfer

Table 2 Thermo-physical properties of paraffin wax and tube materials [12, 23, 24]

Properties	Paraffin wax	Copper tube
Melting point (T_m), K	322	1300
Latent heat of fusion (L), J/kg	243,000	–
Density (ρ), kg/m³	814 (s), 775 (li)	8978
Specific heat (C_p), J/kg K	2160 (s), 2400 (li)	381
Thermal conductivity (k), W/m K	0.35 (s), 0.15 (li)	387
Thermal expansion coefficient (β), 1/K	0.000091	–

inside the copper wall and third term mentions the heat loss / gain from PCM to copper wall.

The outer plastic tube is insulated. Therefore, an adiabatic boundary condition is used as follows,

$$\frac{dT}{dy}\bigg|_{\substack{r=+5\ mm\ to\ 16\ mm,\quad y=0,\quad 300\ mm \\ r=-5\ mm\ to-16\ mm,\quad y=0,\quad 300\ mm}} = 0 \qquad (12)$$

$$\frac{dT}{dr}\bigg|_{\substack{r=+16\ mm,\quad y=0\ to\ 300\ mm \\ r=-16\ mm,\quad y=0\ to\ 300\ mm}} = 0 \qquad (13)$$

2.4 Computational procedure

2-D geometry is created in ANSYS FLUENT 2015. It has an inner copper tube (ϕ 10 mm, thickness 1 mm) and outer plastic tube (ϕ 32 mm) assembly. It is considered that the air flows into the copper tube and PCM is in outer plastic tube. Fine structured mesh is created near the curved edges of copper and plastic tubes to catch enough flow phenomena. The geometry and mesh created are shown in Fig. 2. The pressure based and absolute velocity formulation SIMPLE algorithm is used to solve the momentum and continuity equations. Transient simulations were conducted to capture the velocity, temperature, melting and solidification fractions. Solidification and melting model based on enthalpy-porosity technique is used. Boundary conditions are set at the curved edges of pipes.

The first order upwind scheme is used for solving momentum and energy equations. SIMPLE scheme is used for pressure velocity coupling and PRESTO scheme is used for pressure value at each control volume. Under relaxation factors of 0.5, 0.6, and 0.9 are used for the solution of the momentum equations, the pressure correction equation, and the energy equation, respectively. A finite volume based ANSYS Fluent 2015 tool was used for running the CFD simulations. The liquid fraction was computed and recorded. Liquid fraction region lies in the range 0 to 1 and it is known as mushy zone (discussed later). Modeling of mushy zone is based on 'pseudo' porous medium and it decreases from 1 to 0 while the material solidifies.

2.5 Experimental setup and procedure

The experimental setup for indirect type solar dryer is shown in Fig. 3 (a). It consists of a solar flat plate air collector and drying chamber. Solar collector was provided with a V-shape corrugated absorber plate coated with black paint, simple glass cover and rock wool insulation at the bottom side. A wire mesh tray was used for keeping the material inside the drying chamber. Solar radiation was incident on the glass cover after which a part of the radiation reflects back to the atmosphere while a part passes through the glass cover. After transmission through glass cover, part of the radiation is lost
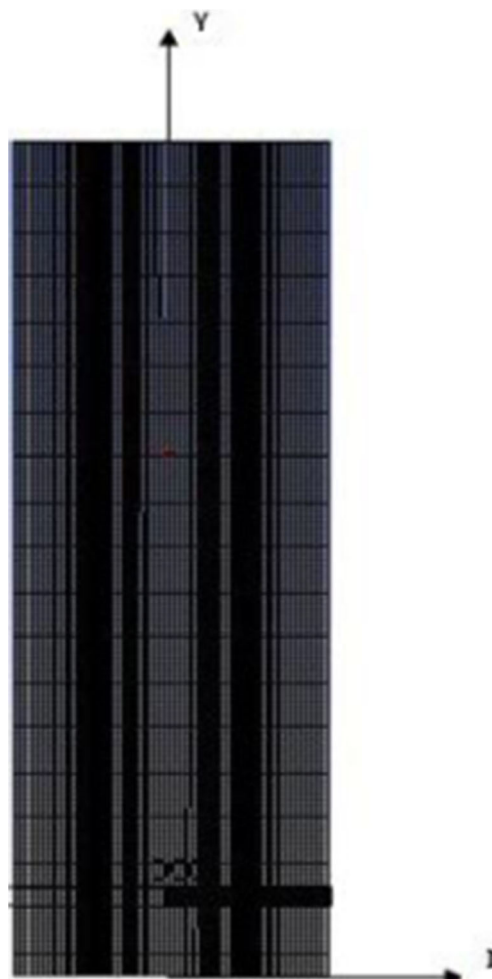

Fig. 2 Geometry and mesh generated for CFD simulation

through a glass cover to atmosphere, while part of radiation is absorbed by absorber plate and the remaining part is transferred by convection to the flowing air. At present there is no TES device in this setup. The input values such as temperature and air velocity were measured from this experimental setup and they were used as inputs for this numerical work. RTD sensors (PT 100, PPI Make, India) were used to measure the collector outlet temperatures (which is assumed as T_{ia} in this numerical work) and a hot wire anemometer (Tenmar TM 207, Taiwan) was used to measure the velocity. Drying experiments were performed on 21st October, 2016. It was found that the velocity range was 1 to 4 m/s and average velocity was 2.5 m/s. Therefore, a velocity range 1 to 4 m/s was chosen for the present numerical work. More details about experimental setup and procedures were explained in the authors' previous work [14].

A proposed setup with TES device and RTD sensor locations are mentioned in Fig. 3 (b). Fresh air enters into the inlet of solar collector plate and gets heated. Then the heated air is allowed to pass through the TES system where a portion of heat is absorbed by the PCM

Fig. 3 **(a)** Experimental setup with solar flat collector and **(b)** Sensors location
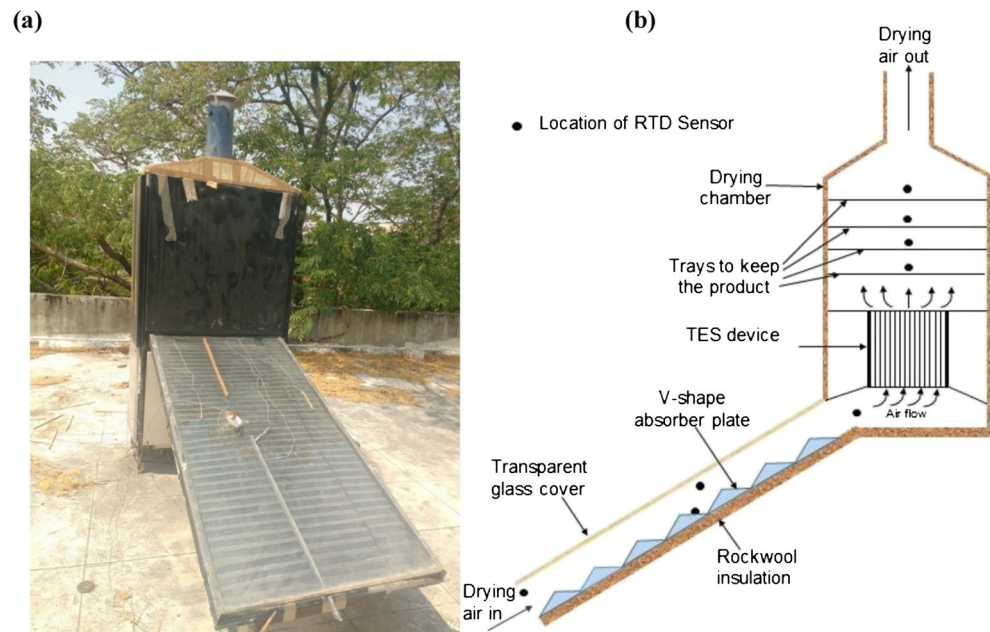
material. The hot air consists of remaining heat enters into the drying chamber of indirect type solar dryer. This hot air is used to remove the moisture from the material inside the drying cabinet. The product moisture content is removed through the opening provided at the top of chamber. In the evening, when solar radiation is reduced, thermal energy stored in the PCM is absorbed by the air and used to dry the material. Therefore, the drying can be continued when there is no sun light.

In the present work, the TES system of indirect type of solar dryer is taken into consideration. This TES device has number of inner and outer tubes. A 2D model is developed for a single set of inner copper tube and outer plastic tube with PCM. Temperature, velocity, melting and solidification fraction are estimated into the TES system.

3 Results and discussions

3.1 Grid independent test

Grid independent test was carried out on three different control voulmes (CVs) 68 × 600, 102 × 600 and 132 × 600. The results were plotted in terms of temperature vs distance from x = 0 to 16 mm at time 300 s (Fig. 4 a). The nature of curve is similar for all the CVs, but the average error between 102 × 600 and 132 × 600 CVs is very low (0.00092%) comparatively the average error between the CVs 68 × 600 and 102 × 600 (0.0021%). Therefore, for the remaining simulations the CVs of 102 × 600 were selected in order to reduce the calculation time.

3.2 Time independent test

Time independent test was carried out on different time steps. The optimized CVs of 102 × 600 were used for this test. This test was carried out at $t = 300$ s on different time steps size 1, 0.75, 0.5 so the total number of time step are 300, 400 and 600 and it was shown in Fig. 4 (b) which shows the variation of temperature with radial distance. The error between the number of time steps 400 and 600 are very less (0.0041%). Therefore, 400 was used as the time step for the remaining simulations.

The temperature variation along the radial distance from the center point is drawn and shown in Figs. 4 (a) and (b). The temperature profile at air section, copper wall and PCM section are plotted. The middle of the air section temperature is higher and it gradually decreases towards the copper wall. This heat is transferred through this copper wall and then it is transferred to PCM through conduction and convection heat transfer.

Melting of PCM is estimated using Eq. (7) and it is compared with the numerical data of Karunesh et al. [12] (Fig. 5). Area weighted average method was used to calculate the melt fraction at equal interval of time. The total time considered is 90 min. As the time increases, melt fraction increases. The present numerical result matches very correctly the result of Karunesh et al. [12]. The average error between the present numerical work and the existing experimental result [12] has been estimated and it is 1.56%.

CFD simulations were performed with optimized grid and time steps. The velocity contour of air which is flown through the copper tube is estimated at 300 s and mentioned in Fig. 6. The inlet velocity considered in this part is 1 m/s. The *Re* is

Fig. 4 (a) Grid and (b) time independent test
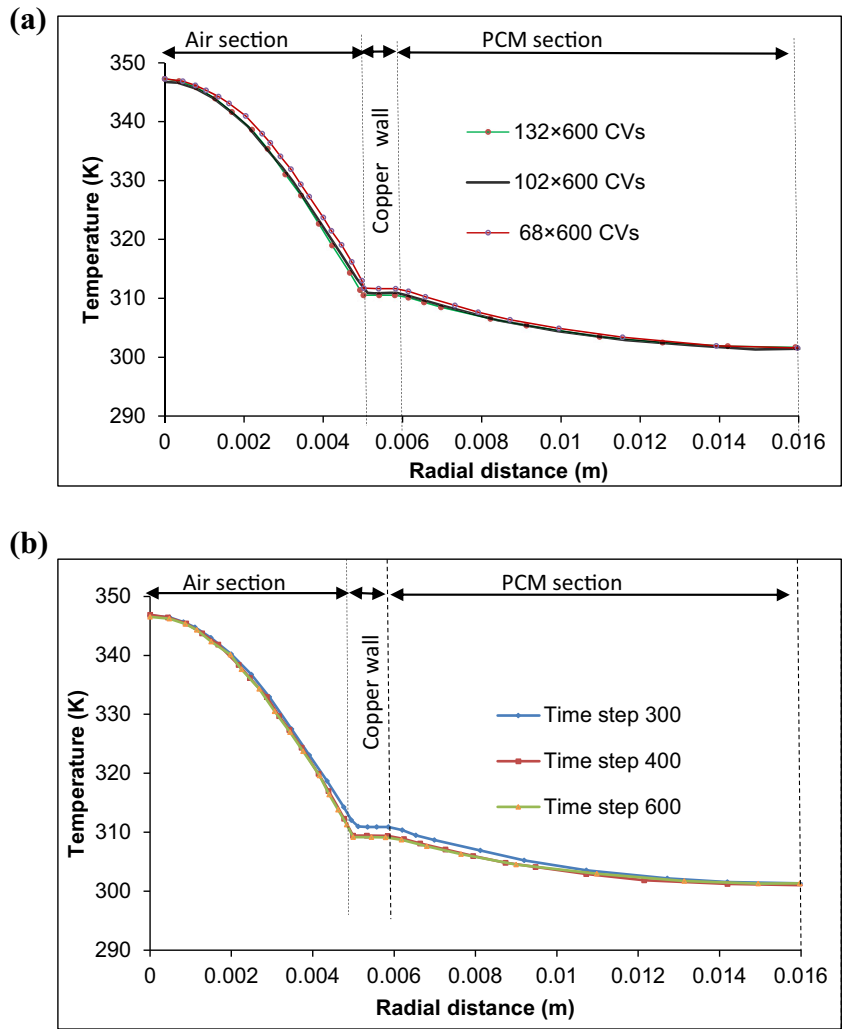
estimated as 432.291, therefore, the flow is considered as laminar. The flow looks almost like a symmetrical profile. The velocity is varied from 0.62 to 1.52 m/s throughout its length. It is observed that the flow is still in a fully developing region.

3.3 Melting and solidification of PCM

Simulations were carried out from 8.00 am to 10.00 pm. First simulation reading was recorded at 8.00 am and the remaining

Fig. 5 Comparison of present numerical work with literature result [12]
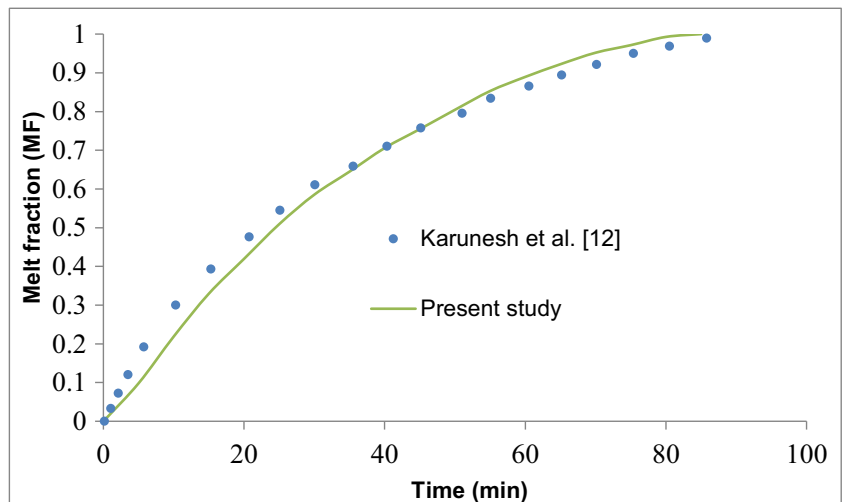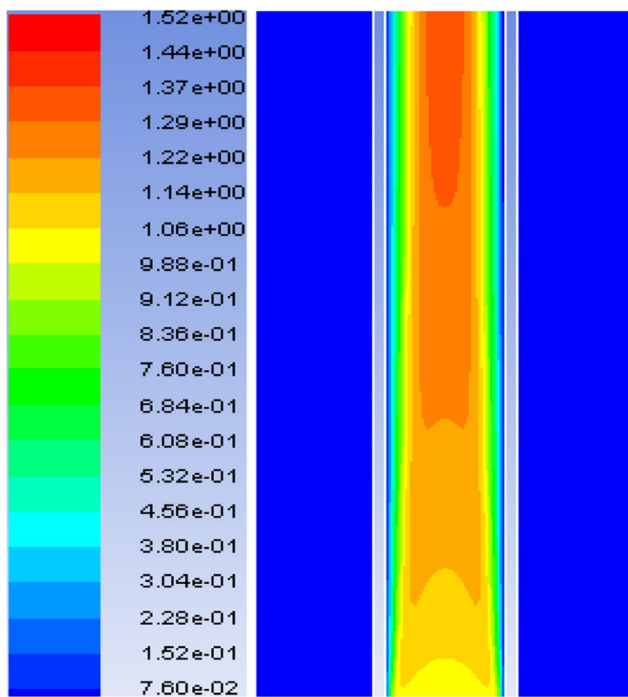
Fig. 6 Velocity contour

reading noted at equal interval of time of one hour and the results are plotted in Fig. 7. Inlet and outlet temperatures were estimated by area weighted average method. It represents the variation of temperature with respect to time at inlet (T_{ia}) and at exit of copper tube (T_{oa}). The T_{ia} is gradually increasing and reaching a maximum value of 349 K at 2.00 pm and at inlet of copper tube. In this simulation different air velocities have been chosen (1, 2, 3 and 4 m/s) to check the outlet temperature of air (T_{oa}). At 1 m/s, T_{oa} reaches a maximum value of 341 K at 2.30 pm and then it decreases as the solar radiation falls. The exit temperature of air (T_{oa}) which is the inlet of drying chamber gradually increases from 308 K at 8.30 am to 341 K at 2.30 pm. Up to this time region, T_{oa} is lesser than T_{ia}
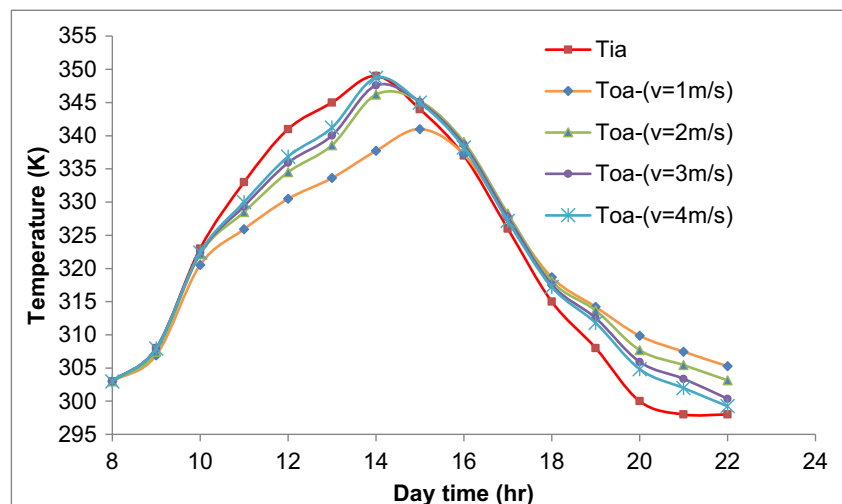
because of heat loss to the PCM. After this region T_{oa} is found to be gradually decreasing but it is still greater than T_{ia}. For example, at 6.00 pm, T_{ia} is 315 K, but T_{oa} is 319 K and at 10.00 pm, T_{ia} is 298 K, but T_{oa} is 305.3 K. It proves that the air is taking latent heat energy from PCM when there is no sunshine. Thus T_{oa} is more than T_{ia} and it maintains the drying chamber temperature higher than the environmental air. From Fig. 8 it is observed that from 4.00 pm to 10.00 pm, average T_{oa} is 317 K and that of the T_{ia} is 307 K. So it is possible to maintain the average temperature of 10 K more than the atmospheric using TES at the air velocity of 1 m/s. The minimum inlet air temperature (T_{ia}) is noticed as 298 K at 10.00 pm (Fig. 7).

The device outlet temperatures are also tested at other three velocities 2, 3 and 4 m/s (Fig. 7). The maximum outlet temperatures (T_{oa}) are noticed at 2.00 pm as 346, 347.6 and 348.7 K at different air velocities 2, 3 and 4 m/s, respectively. Therefore, if the air velocity inside the copper tube is increased, maximum T_{oa} is reached at maximum T_{ia} value. If air flow velocity is increased, then the convection heat transfer is increased, and hence the maximum temperature also increases and reaches its maximum T_{ia} value. The average temperatures of T_{oa} at 4.00 to 10.00 pm are varied as 317 K, 316.5 K, 315.2 K and 314.4 K at different air flow velocities from 1 to 4 m/s. Average of T_{oa} at 4.00 to 10.00 pm at different air velocities from 1 to 4 m/s is 316 K, which is greater than the average of T_{ia} (311 K) of the same time range. Therefore, a minimum of 5 K temperature difference is seen in the case of T_{oa} and T_{ia}, so the drying process can be performed upto 10.00 pm at any air flow velocities. At 10.00 pm the available T_{oa} are 305.3 K, 303.2 K, 300.4 K and 299.3 K at different velocities - 1, 2, 3 and 4 m/s, respectively. This temperature is enough to dry the food materials. Therefore, it is proved that by using this TES device, the drying experiments can be performed upto 10.00 pm.

Fig. 7 Variation of inlet temperature (T_{ia}) and outlet temperature (T_{oa}) during day time

Fig. 8 Melt fraction variations with respect to time and at different velocities
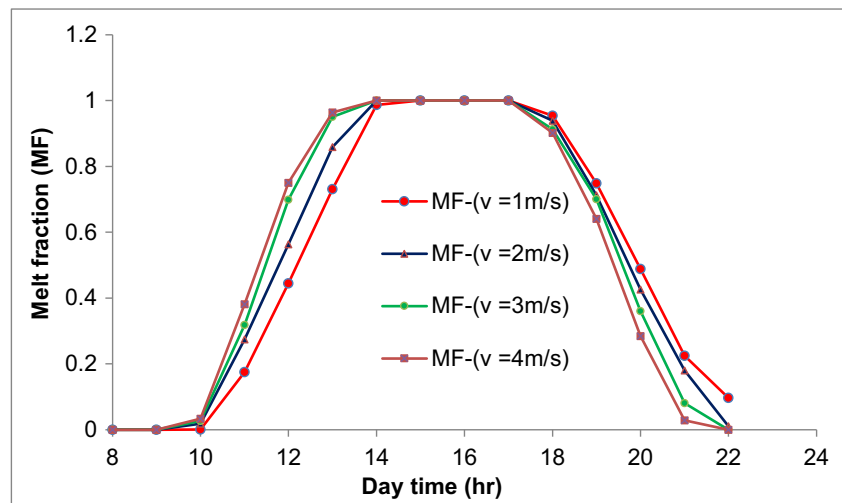
Melt fraction of PCM is drawn at each hour and at different air flow velocities from 1 to 4 m/s and it is shown in Fig. 8. The variation is taken from 8.00 am to 10.00 pm. The air flow velocity of 1 m/s is explained in this paragraph. It is observed that the temperature at 8.00 am is not enough to melt the PCM through copper wall interface so zero melting fraction is found. It continues up to 10.00 am. After this time the PCM (paraffin wax) starts to melt as it reaches its melting point temperature of 322 K (49 °C) (which is already explained in Fig. 7). The melt fraction gradually increases as time progresses and it reaches 1 (fully melted) at 2.00 pm and it continues for up to 5.00 pm. During this time, the PCM absorbs maximum heat energy from hot air. After 5.00 pm the melt fraction started to decrease as the temperature decreases further with time (which was explained in Fig. 7). Up to 6.00 pm the decrease happened in a slow manner and after 6.00 pm it was vigorous as the air temperature drops to 300 K or even less as time progresses to evening.

An almost similar variation was noticed at higher velocities from 2 to 4 m/s. The melt fraction gradually increases and reached a fully melted stage (melt fraction = 1) at 2.00 pm and it was maintained for up to 5.00 pm for all velocity ranges. At 10.00 am, the melt fraction is 0.008% at a velocity of 1 m/s and it is increased to 1.87%, 2.7 and 3.36% for other higher velocities 2, 3 and 4 m/s respectively. Similarly melting fraction at 1 pm is observed as 73.04%, 85.91%, 95.08 and 96.40% at different air velocities of 1, 2, 3 and 4 m/s, respectively. As the heat transfer coefficient between the hot air and the copper plate is a strong function of air velocity, therefore the velocity of air increases, the melting fraction of PCM increases through convection heat transfer.

Solidification process starts at approximately 6.00 pm at all velocities considered in this study. At 9.00 pm (21 h in Fig. 8) the melt fraction is observed as 22.45%, 18.06%, 8.08 and 2.84% at velocities of 1, 2, 3 and 4 m/s, respectively. It means that solidification fraction is increased at 77.95%, 81.94%,

91.92 and 97.16% at different air flow velocities of 1, 2, 3 and 4 m/s and at 9.00 pm. As the air flow velocity increases, the PCM is losing its sensible heat to flowing air in copper tube because the air temperature is less at 9.00 pm. Therefore, at a given temperature the melting and solidification processes are fast during the higher air flow velocities. It is observed that the air flow velocity of 1 m/s is good for maintaining outlet air temperature (T_{oa}) for a long time as compared to other higher velocity conditions.

The temperature distribution of TES device along the horizontal distance is plotted in Fig. 9 at different times. It shows the temperature distribution of three regions such as air, copper wall and PCM section. It is plotted from one half of TES device (or from center of the domain developed for this study) as the coordinate axis is fitted at the center of the problem domain. It is noticed that the temperature decreases from the center of air region. The temperature gradient from center to surface is noticed as 3.7 K at 10 am. And it is varied as 15.9, 17.16 and 15 K at 11.30 am, 12.30 pm and 1.00 pm, respectively. In the copper wall region the constant temperature is maintained because of its higher thermal conductivity and its small thickness (1 mm). This heat is transferred to PCM region and the temperature further decreases because the heat is conducted from the copper wall and to the PCM material. The average temperature of PCM increases from 10.00 am to 2.00 pm as shown in Fig. 9.

Figure 10 shows the variation of average PCM temperature during charging (heat gain) and discharging (cooling) throughout the day. An area weighted average method was used to estimate PCM temperature. It is observed that the paraffin wax stores heat energy in terms of both sensible and latent heat. The temperature of PCM gradually increases from 304 to 318 K from 8.30 am to 10.00 am because the PCM stores the heat energy through sensible heat. Similarly, at 3.00 pm the temperature is raised to its maximum value 338.3 K. After this time (at 3.00 pm) the sun-shine falls and

Fig. 9 Variation of temperature during heating (charging) at different time and at the velocity of 1 m/s
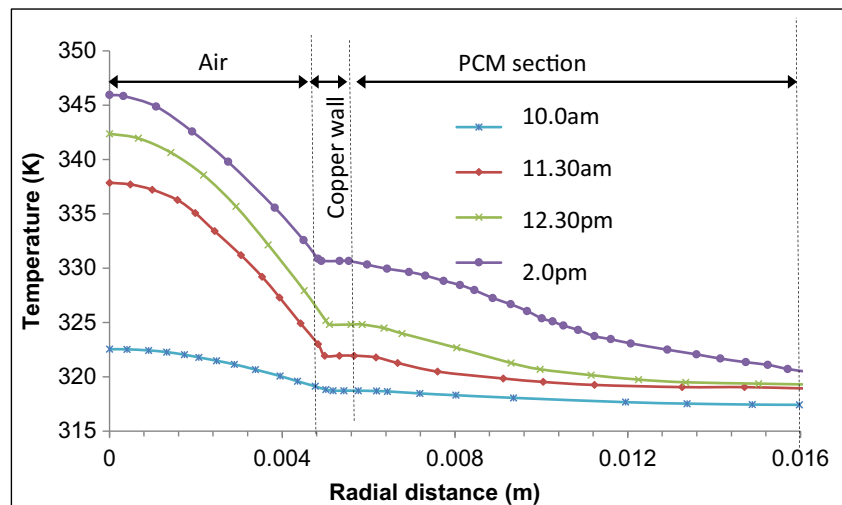

PCM loses much of the heat energy to moving air and hence the temperature of PCM falls. At 5.30 pm, the temperature dropped to 322 K. Paraffin wax's melting temperature is 322 K; therefore from 1.00 pm to 5.30 pm, the PCM is in liquid phase and at other times it solidifies. The temperature further dropped (316 K) at 9.30 pm. This is greater than the temperature of room air (298 K room air at 9.30 pm). Therefore, even at late night the air is heated by the heat energy of PCM. It proves that there is a chance of drying of agricultural products round the clock using the temperature of hot air in the drying chamber, with temperatures above the room temperature.

Temperature distribution during the heating (charging) of PCM at different times is shown in Figs. 11 (a), (b) and (c). The initial temperature of PCM is considered at 300 K. The maximum temperature is noticed at the inlet of the copper pipe and it is varied from 341 to 349 K when time varies from 11.30 am to 2.00 pm. At the starting hours of melting, at 11.30 am, the temperature distribution in PCM is 319 K (Fig. 11 a) and it increases because it is absorbing energy from

hot air. At 11.30 am a major portion of the PCM's temperature is in the range of 320 K (Fig. 11 a). It is absorbing heat energy from hot air when time progresses and therefore, the major temperature change is noticed in the range of 324 to 330 K at 12.30 pm and it is shown in Fig. 11 (b). At 2.00 pm almost all the regions of PCM temperature reaches up to 332 K (Fig. 11 c). Therefore the PCM melts as it reaches its melting point temperature (322 K) and this melting phenomenon is discussed in the next paragraph. The average temperature in the PCM (Fig. 10) is obtained as 318.26 K, 320 K, 321.32 K, 323.77 K and 333.23 K at 10.00 am, 11.30 am, 12.30 pm, 1.30 pm and 2.00 pm, respectively, and at an air velocity of 1 m/s.

The melt fraction distributions of PCM over different times are shown in Fig. 12. Area weighted average is taken for each time zone. At 10.00 am (Fig. 12 a) the PCM did not melt (or its average value is very low and it is noticed as 0.00007929 or 0.008%) because the average temperature of PCM is 319.5 K which is below its melting temperature (322 K). In the next stage (at 11.30 am, Fig. 12 b) melting started at the layer close

Fig. 10 Average temperature of PCM throughout the day (charging and reuse) at 1 m/s
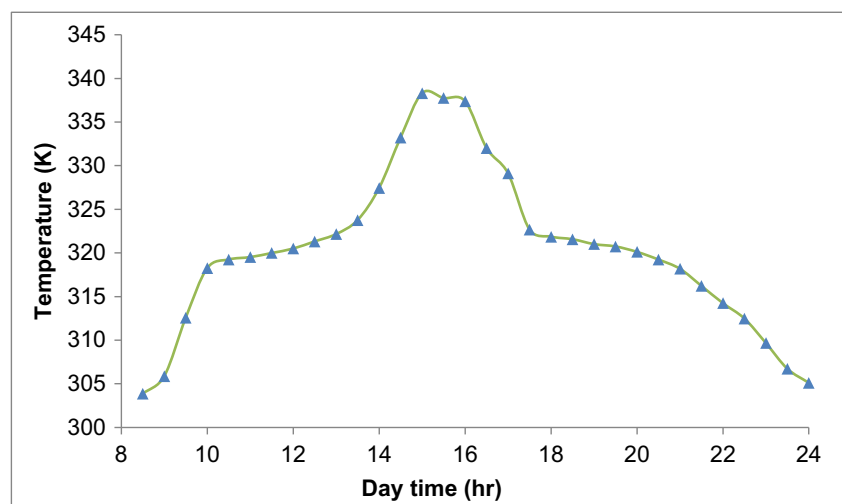
to the copper wall, because the wall temperature is higher than the melting point of PCM at this stage. The average melting point is noticed as 0.318 at 11.30 am because the temperature near the copper wall is approximately 326 K (explained in Fig. 11 a). As the time increases the solar radiation also increases; therefore, the collector outlet air temperature also increases. The copper absorber tube absorbs the heat energy from hot air and from the copper tube the heat is transferred to PCM material through convection heat transfer.

The average melting fraction value is increased to 0.5913 at 12.30 pm (already explained in Fig. 8) and distribution of melt fraction is shown in Fig. 12 (c). At the outlet region, the melting fraction of PCM looks like a funnel on the graph because at the curved edge the heat transfer coefficient values are maximum due to higher impact of hot air on the edge compared with other surfaces. It makes the temperature higher at outlet (Fig. 11 a) and also the melting fraction higher near the outlet edge (Fig. 12 c).

At 2.00 pm (Fig. 12 d) 99% (as shown in Fig. 8) of melting is completed because the average temperature of PCM noticed is 327 K. The entire PCM melts and the average temperature reaches 327 K at 2.00 pm and 338.32 K at 3 pm. (Fig. 8). Therefore, it can be concluded that at these two time zones the energy stored by the PCM is maximum. At 10.00 am, 0.79% melting has taken place and it further increased to 31.8% at 11.30 am, 59.13% at 12.30 pm and 99% at 2.00 pm, respectively.
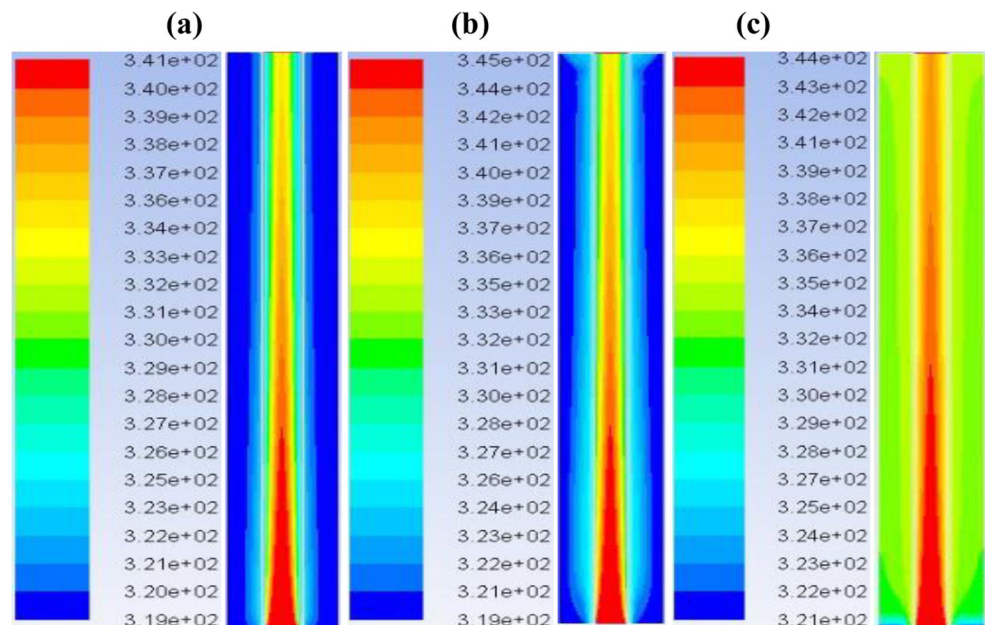
3.4 Solidification of PCM

In this section the variation of temperature and solidification factor of PCM are discussed. During this time the PCM cools down and therefore the stored energy by PCM is re-used for possible agricultural products' drying when the sun shine is off or when there is no sunlight. Therefore, it is possible to achieve the drying process even when there is no sun light as the drying chamber temperature can be maintained at more than the inlet air temperature (T_{ia}).

Figure 13 shows the variation of temperature during the cooling of PCM. It is noticed that the air and PCM temperature gradually dereases when the time increases towards the sun shine-off. At 5.30 pm the air temperature drops to 315.7 K, but the copper wall temperature is 322 K. Now the copper wall is obsorbing the heat energy from PCM (which is exactly reversed) as the maximum PCM temperature is more (324.4 K). The temperature of air drops again to 309.2 K at 7.00 pm, 301.6 K at 8.00 pm and 300 K at 9.00 pm. But maximum temperature of PCM is almost constant (322.3 K) for all the above mentioned time regions. The average temperature of PCM is more than 322 K at 5.30 pm. But at other times periods mentioned in the study (7.00 pm, 8.00 pm and 9.00 pm) the temperature remains below 322 K, therefore the PCM starts to solidify. This solidification factor is explained in the next paragraph. For all the time regions here, the stored heat energy is conducted to copper wall and then again the heat is transferred to the flowing air in the copper tube. It is concluded that the air temperature during sun shine-off time is always greater than the inlet air temperature (T_{ia}). Therefore, the energy storage facilty in drying setups can give better performance for dryers and the drying process can be performed round the clock.

Temperature distribution during the cooling of PCM is estimated at different times and shown in Figs. 14 (a), (b) and (c). The cooling of PCM starts near the copper wall during sun shine-off time and the cooling front moves slowly towards the end side of the PCM wall. That means that the PCM loses heat

Fig. 11 Temperature contour during heating (charging), at (a) 11.30 am, (b) 12.30 pm and (c) 2.00 pm and at air velocity of 1 m/s
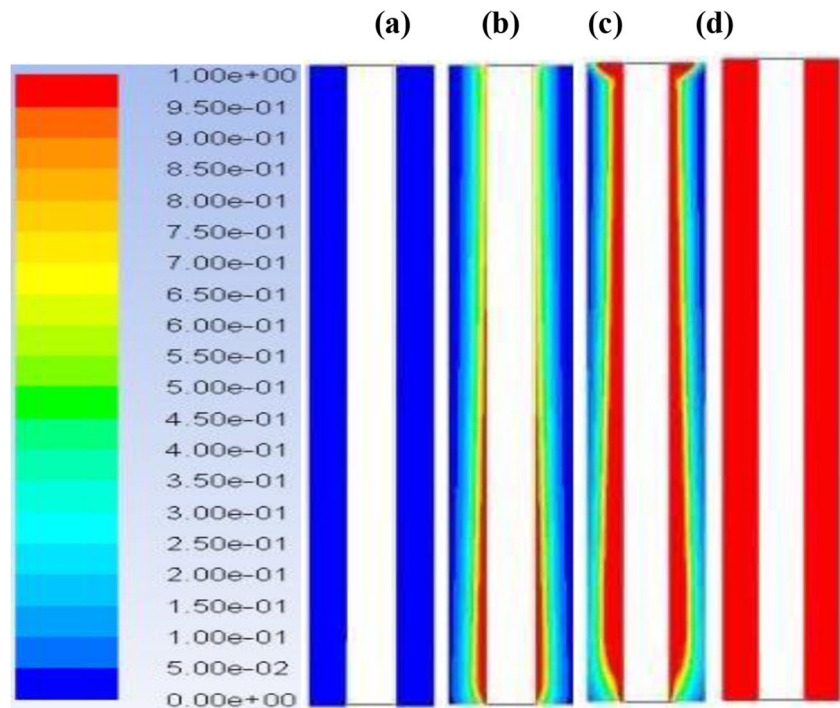
near the copper wall and therefore the heat is always conducted from the interior nodes to nodes near the copper wall. Fig. 14 (a) shows the temperature distribution of TES device at 5.30 pm. The maximum temperature and average temperature of PCM are noticed 325 and 321.1 K (as already explained in Fig. 10), respectively. Therefore, the PCM is still in molten state, but a portion of PCM starts solidifying (at 7.00 pm, Fig. 14 b) when the time progresses and the temperature drops below the melting temperature of 322 K. The average temperature of PCM in this case is 315 K.

At 9.00 pm, the temperature of PCM near the copper wall is reduced to 315 K therefore major portion of the the PCM solidifies and it is shown in Fig. 14 (c). But still the heat energy is transferred to the flowing air in the copper tube as the air temperature is less (308 K) compared to the PCM temperature. Overall, when the sun shine is off after

5.30 pm, the air temperature drops and the copper wall acts as a cooling source. This is the reason the PCM near the copper wall cools down first and subsequently heat is conducted from outer surface to inner surface of PCM and hence the PCM starts to solidify. But PCM is always transferring the heat to the air because the air temperature is still less (308 K). From this analysis it is observed that the temperature difference between the air inlet and outlet is a maximum of 12.6 K during peak solar radiation time and the minimum is 5 K during the sun shine-offtime. The average temperature in the PCM during the solidification (Fig. 10) is obtained as 322.68 K, 321.86 K, 321.01 K, 320.12 K, 318.18 K at 5.30 pm, 6.00 pm, 7.00 pm, 8.00 pm and 9.00 pm, respectively.

The solidification phenomenon of PCM is shown in Fig. 15 at different sun shine-off times. This is the process of discharging the stored thermal energy from PCM and this thermal energy is re-used for useful work for continuous drying of food products. Solidification of PCM starts when the temperature at the inlet to TES device (T_{ia}) is less than the temperature of melted PCM. At 5.30 pm, almost all the region of PCM becomes molten liquid (Fig. 15 a) because of the reason that the PCM temperature is more than its melting temperature, as already discussed in Fig. 14 (a). Fig. 15 (b) is plotted at 6.00 pm. Now the T_{ia} drops and therefore the surface near the copper wall gets cooled. The PCM loses heat near the copper wall to below its melting point temperature and hence solidification starts. The solidification is gradually increased when the time progresses to 7.00 pm (Fig. 15 c), 8.00 pm (Fig. 15 d) and 9.00 pm (Fig. 15 e). But the PCM
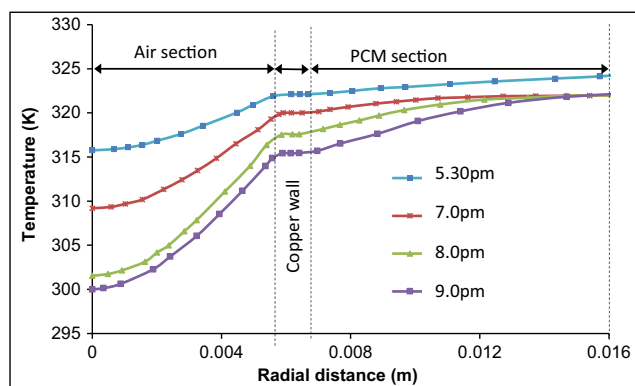
**Fig. 13** Variation of temperature during cooling (reuse)
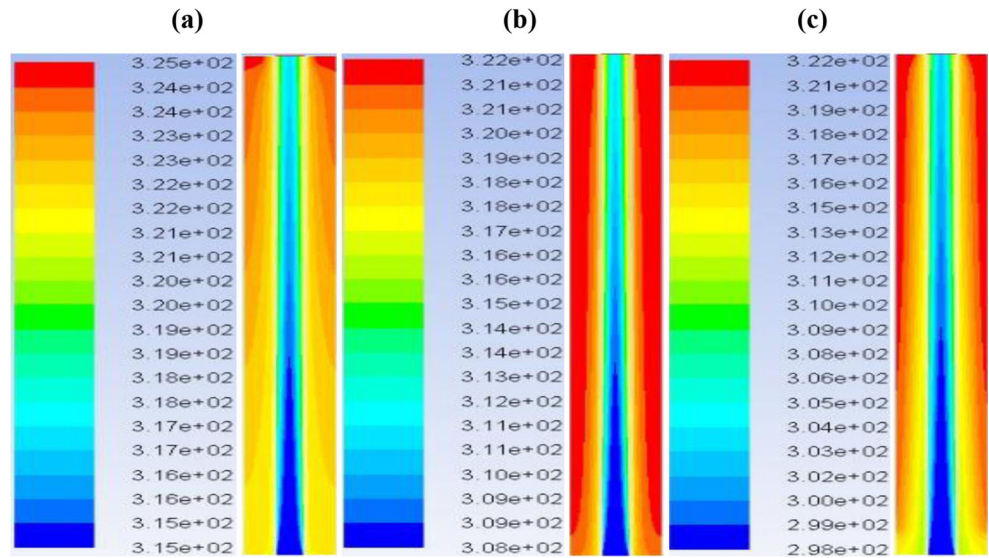
temperature is always higher than the air temperature which is to be supplied to the drying chamber. Therefore, it is concluded that after 5.00 pm solar radiation is not sufficient to dry the product, but due to TES device, the stored energy is utilized by air therefore, T_{oa} is more than T_{ia}.

The heat stored and released by PCM are calculated based on heat loss and gain by air with respect to time and it is shown in Fig. 16. Heat loss or gain were calculated using $mC_p(T_{oa} - T_{ia})$, where, m is mass of air entering inside the setup, C_p is specific heat of air, T_{oa} and T_{ia} are outlet and inlet air temperatures. The heat transfer from inlet air to TES device is taken as heat lost by air. When there is no sunlight, heat is transferred from TES device to air is taken as heat gain by air. Simulations are started from 8.00 am. Initially the heat transfers from inlet

air to PCM, therefore air loses its heat. At air flow velocity 1 m/s, this heat loss of air is increased and reached a maximum value of 3534 J and then it is started to decrease when sunlight is decreased. The maximum and minimum heat stored in TES device at 12.00 pm are noticed as 5175 J and 3233 J at air velocity 4 m/s and 1 m/s respectively (Fig. 16). After 4.00 pm, the air gets heat from PCM as the sunlight is dropped further at 1 m/s. This heat gain is increased and reached a maximum value of 3304 J and then started to decrease as there is an equilibrium achieved in between the heat of PCM and air inlet. Similar variation is found on all other velocity considered in this work. The maximum heat gain by air is varied as 5126, 5867 and 6328 J for different air flow velocity 2, 3 and 4 m/s respectively.
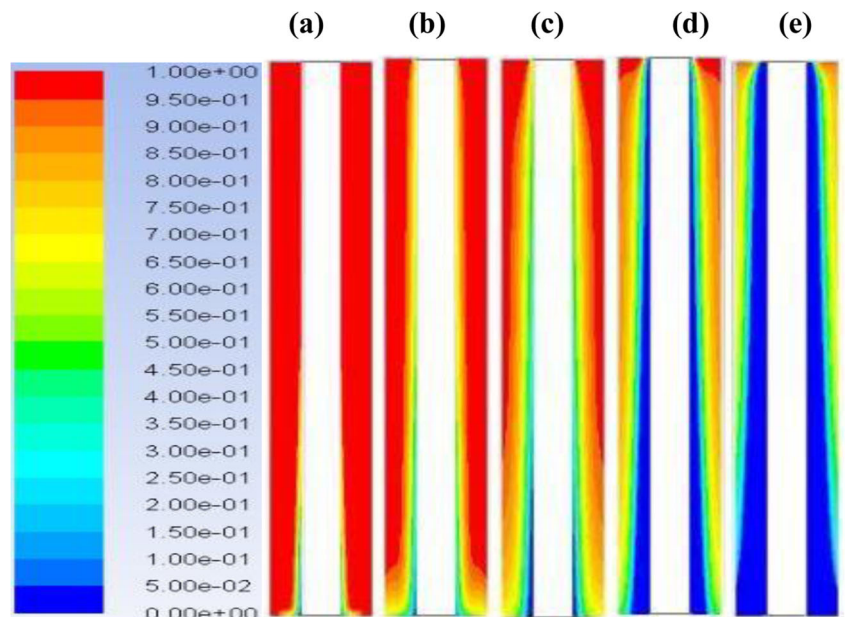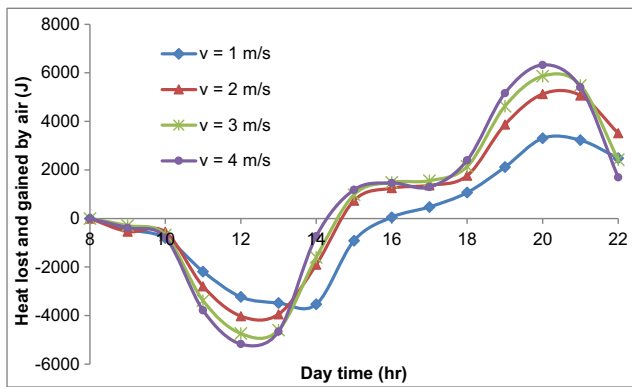
Fig. 16 Heat lost and gained by air with respect to time

4 Conclusions

In this study, a two-dimensional numerical model was developed for thermal heat storage system of an indirect type solar dryer provided with paraffin wax as heat storage material. The melting and solidification behavior of PCM were predicted using the finite volume based CFD tool ANSYS Fluent 2015. The input temperature and velocity ranges were determined from experimental results. Grid and time independent study were performed to identify the optimum number of grids and time steps. The present results were compared with results from existing literature and it was remarkable that the results were in good agreement.

The CFD simulations were run from 8.00 am to 10.00 pm. The inlet air temperature (T_{ia}) was gradually increased and reached a maximum value of 349 K at 2.00 pm. During the sun shine-off time, the outlet temperature of air (T_{oa}) was more than T_{ia}, because the air always takes the heat energy from PCM (paraffin wax). It was observed that the paraffin wax was storing and releasing (charging and discharging) the latent and sensible heat. The average T_{oa} value was 10 K more than T_{ia} during 4.00 pm to 10.00 pm at an air velocity of 1 m/s as the PCM gave more heat energy to air. Also, the average T_{oa} was 5 K more than T_{ia} during 4.00 pm to 10.00 pm at different air velocities (1 to 4 m/s) considered in this work; therefore the drying process can continue for up to 10.00 pm for any air velocity conditions.

The melting of PCM started at 10.00 am (approximately) under all velocity conditions considered in this work (1 to 4 m/s) because the PCM reached its melting temperature of 322 K. Also, all velocity conditions of 1 to 4 m/s, the PCM reached its fully melted condition at 2.00 pm as this span of time had high solar radiation and it was maintained until 5.00 pm because the PCM absorbed maximum heat energy from hot air. At a particular time, during the heating process, the melting fraction of PCM was increased with increased air flow velocities as heat transfer coefficients between the air with copper wall and PCM with copper wall played a major role. Similarly, during the cooling process, the solidification fraction

increased with increased air flow velocities, because of the domination of convection phenomena. The air flow velocity at 1 m/s was good for maintaining long time T_{oa}, compared to other velocities. Heat lost and gained by air was estimated from 8.00 am to 10.00 pm. Air velocity dominated the heat lost and gained by air during the process. Maximum heat gained was noticed as 6328 J at air velocity 4 m/s.

The proposed TES model with paraffin wax is useful to analyze the potential of PCM to store excess solar energy during sunshine hour and releasing the same in sun shine-off time. The model also helps us to estimate the temperature distribution in radial direction of TES device.

Highlights
- A numerical model is developed for the TES system of an indirect type solar dryer.
- Average drying chamber temperature is 10 K more than the ambient at 1 m/s and 5 K at other velocities.
- The PCM starts to melt at 10 am, fully melts at 2 pm and continues up to 5 pm.
- Air velocity 1 m/s is good to maintain long chamber temperature in drying chamber.
- The drying can be continued up to 10 pm with the help of paraffin wax as a PCM.

Compliance with ethical standards

Conflict of interest On behalf of all authors, the corresponding author states that there is no conflict of interest.

Publisher's Note Springer Nature remains neutral with regard to jurisdictional claims in published maps and institutional affiliations.

References

1. Shalaby SM, Bek MA (2014) Experimental investigation of a novel indirect solar dryer implementing PCM as energy storage medium. Energy Convers Manag 83:1–8
2. Zhao W, France DM, Yu W, Kim T, Singh D (2014) Phase change material with graphite foam for applications in high-temperature latent heat storage systems of concentrated solar power plants. Renew Energy 69:134–146
3. Ayyappan S, Mayilsamy K, Sreenarayanan VV (2016) Performance improvement studies in a solar greenhouse drier using sensible heat storage materials. Heat Mass Transf 52(3):459–467
4. Baniasadi E, Ranjbar S, Boostanipour O (2017) Experimental investigation of the performance of a mixed-mode solar dryer with thermal energy storage. Renewable Energy 112:143–150

5. Cakmak G, Yidiz C (2011) The drying kinetics of seeded grape in solar dryer with PCM-based solar integrated collector. Food Bioprod Process 89:103–108

6. Tekasakul P, Kumar A, Yuenyao C, Kirirat P, Prateepchaikul G (2017) Assessment of sensible heat storage and fuel utilization efficiency enhancement in rubber sheet drying. J Energy Storag 10: 67–74

7. Arasu AV, Mujumdar AS (2012) Numerical study on melting of paraffin wax with Al2O3 in a square enclosure. Int Comm Heat Mass Transfer 39(1):8–16

8. Lafdi K, Mesalhy O, Elgafy A (2008) Graphite foams infiltrated with phase change materials as alternative materials for space and terrestrial thermal energy storage applications. Carbon 46:159–168

9. Dutil Y, Nizar DRR, Salah B, Lassue S, Zalewski L (2011) A review on phase-change materials: mathematical modeling and simulations - a review. Renew Sust Energ Rev 15:112–130

10. Sharma SD, Sagara K (2005) Latent heat storage materials and systems: a review. Int J Green Energy 2(1):1–56

11. Khodadadi JM, Hosseinizadeh SF (2007) Nanoparticle-enhanced phase change materials (NEPCM) with great potential for improved thermal energy storage. Int Commun Heat and Mass Transfer 34(5): 534–543

12. Karunesh K, Shukla A, Sharma A (2016) Performance evaluation of fatty acids as phase change material for thermal energy storage. J Energy Storag 6:153–162

13. Yang L, Peng H, Ling X (2015) Numerical analysis on performance of naphthalene phase change thermal storage system in aluminum plate-fin unit. Heat Mass Transf 51(2):195–207

14. Abhay L, Chandramohan VP, Raju VRK (2017) Design, development and performance of indirect type solar dryer for banana drying. Energy Procedia 109:409–416

15. Arunsandeep G, Abhay L, Razatkumar N, Chandramohan VP, Raju VRK (2017) Numerical solution and it's analysis during solar drying of green peas. J Inst Eng (India): Series C:1–9. DOI https://doi.org/10.1007/s40032-017-0379-5

16. Chandramohan VP, Talukdar P (2010) Three dimensional numerical modeling of simultaneous heat and moisture transfer in a moist object subjected to convective drying. Int J Heat Mass Transfer 53: 4638–4650

17. ChandramohanVP TP (2013) Design of an experimental set up for convective drying: experimental studies at different drying temperature. Heat Mass Transf 49(1):31–40

18. Chandramohan VP, Talukdar P (2014) Experimental studies for convective drying of potato. Heat Transfer Eng 35(14):1288–1297

19. Ateeque M, Udayraj, Mishra RK, Chandramohan VP, Talukdar P (2014) Numerical modeling of convective drying of food with spatially dependent transfer coefficient in a turbulent flow field. Int J Ther Sci 78:145–157

20. Razatkumar N, Arunsandeep G, Chandramohan VP (2017) Numerical simulation for freeze drying of skimmed milk with moving sublimation front using tri diagonal matrix algorithm. J Appl Fluid Mech 10(3):813–818

21. Robert RC, Thomas SK (1996) The properties of gases and liquids. McGraw Hill, New York

22. Brent AD, Voller VR, Reid AJ (1998) Enthalpy-porosity technique for modeling convection diffusion phase change: application to the melting of a pure metal. Numerical Heat Transfer 13:297–318

23. Humphries W, Griggs E (1977) A design handbook for phase change thermal control and energy storage devices, NASA Technical Paper 1074 NASA Scientific and Technical Information Office

24. Inaba H, Tu P (1997) Evaluation of thermophysical characteristics on shape-stabilized paraffin as a solid-liquid phase change material. Heat Mass Transf 32(4):307–312